

UNIVERSIDADE ESTADUAL DE CAMPINAS
SISTEMA DE BIBLIOTECAS DA UNICAMP
REPOSITÓRIO DA PRODUÇÃO CIENTÍFICA E INTELLECTUAL DA UNICAMP

Versão do arquivo anexado / Version of attached file:

Versão do Editor / Published Version

Mais informações no site da editora / Further information on publisher's website:

<https://www.sciencedirect.com/science/article/pii/S2215038215300406>

DOI: 10.1016/j.colcom.2016.03.003

Direitos autorais / Publisher's copyright statement:

©2016 by Elsevier. All rights reserved.

DIRETORIA DE TRATAMENTO DA INFORMAÇÃO

Cidade Universitária Zeferino Vaz Barão Geraldo

CEP 13083-970 – Campinas SP

Fone: (19) 3521-6493

<http://www.repositorio.unicamp.br>



Rapid Communication

Mapping of heterogeneous wetting inside superhydrophobic coatings

Omar Teschke^{a,*}, Wyllerson Evaristo Gomes^a, David Mendez Soares^a, Elizabeth Fatima de Souza^b^a Laboratório de Nanoestruturas e Interfaces, Instituto de Física, UNICAMP, 13083-859 Campinas, SP, Brazil^b CEATEC – Faculdade de Química – PUC-Campinas, 13086-900 Campinas, SP, Brazil

ARTICLE INFO

Article history:

Received 3 September 2015

Received in revised form 7 March 2016

Accepted 22 March 2016

Available online 11 April 2016

Keywords:

Heterogeneous wetting profiles

Capillary evaporation

PECA superhydrophobic coatings

Kelvin equation

ABSTRACT

The condition for the occurrence of induced drying inside structured coating was calculated and corresponds to a new format of the Kelvin equation. Water spatial distribution inside immersed interconnected fibers forming superhydrophobic coatings was then imaged by confocal Raman microscopy characterizing the heterogeneous wetting profile. Coatings were structurally characterized by scanning electron microscopy (resolution $\sim 0.1 \mu\text{m}$) and interconnected fiber structure lateral area and empty volume (V_{emp}) measured. The combination of these micrograph images yield a new measurement technique readily applied for structurally characterizing immersed coating hydrophobicity. When this technique was applied for coatings showing induced drying, the measured coating layer lateral area per unit volume was $\sim 10^4/\text{m}$, which differs by two orders of magnitude with the value calculated by the Kelvin equation.

© 2016 Elsevier B.V. All rights reserved. This is an open access article under the CC BY-NC-ND license (<http://creativecommons.org/licenses/by-nc-nd/4.0/>).

The investigation of how water interacts with hydrophobic solids is crucial for understanding many natural and technological phenomena [1,2]. Hydrophobic units do not hydrogen bond to water. This loss of hydrogen bonding near hydrophobic surfaces may cause water to move away from those surfaces and produce vapor layers [3]. While it is generally believed that vapor is trapped at the interface between water and superhydrophobic surfaces, direct experimental evidence for the presence of vapor at the microscopic level is rare [4]. Recently new methods for the observation of nanobubbles were developed as total internal reflection and optical interference enhanced reflection [5,6]. Capillary drying [7], Cassie state wetting [8], dewetting [9,10], superhydrophobicity on hairy surfaces [11] are now areas of intense investigations.

Induced drying could occur inside complex, interconnected structures of nanofibers immersed in water, as described here. Volumetric considerations can aid in the prediction of this effect: the bound water has a surface energy equal to the product of the lateral surface area and the interfacial tension. This energy is opposed by the bulk free energy, which is defined as the product of the average number of bound water molecules and the difference in the chemical potentials of liquid water and water vapor. On the other hand, for large empty spaces between structures, the bulk energy dominates over the surface energy, and thus the bound water is stable. On the other hand, when the film is highly structured, the surface energy is dominant, and bound water is destabilized with respect to water vapor. Comparison of the energies of bulk water and surface water provides an estimate for the range of surface structure empty volume in which this effect will become significant. This comparison is derived by equating the grand potential of

confined water $\Omega_w \approx -PV_{\text{emp}} + A_{\text{lat}} \cdot \gamma_{\text{latw}}$ [3] with that of confined vapor $\Omega_v \approx -P_v V_{\text{emp}} + A_{\text{lat}} \cdot \gamma_{\text{latv}} + \gamma A$, where V_{emp} is the volume of the empty region inside the coating, A_{lat} is the lateral area of the structure and A is the top water-vapor interface area. The γA term is negligible because of the top coating surface area in contact with the liquid is much smaller than the coating structure lateral surface area. For an incompressible fluid such as water, the difference between the bulk pressure P and the pressure of the coexisting vapor P_v is approximated by $\rho \Delta\mu$, where ρ is the number density of water and $\Delta\mu$ is the difference between the chemical potential of bulk water and of water-vapor coexistence, resulting in the Kelvin equation. We used the Young–Dupre equation $\gamma \cos \theta = \gamma_{\text{latv}} - \gamma_{\text{latw}}$ [12] to relate the difference in surface tension between coating/vapor (γ_{latv}) and coating/water (γ_{latw}) to the surface tension of the water/vapor interface γ and the contact angle θ .

For highly structures film, the coating volume $V \approx V_{\text{emp}}$ and the Kelvin equation is rewritten as

$$A_{\text{lat}} = \frac{-\rho \Delta\mu}{\gamma \cos \theta} \quad (1)$$

where A_{lat} is the coating lateral area per unit volume. So induced drying occurs inside interconnected structure of nanofibers immersed in water when the coating lateral per unit volume is given by Eq. (1). Kelvin equation is usually associated with the surface free energy of a forming liquid drop. More recently an expression was derived for induced drying in large flat surfaces [13]. Here a new format of the Kelvin equation where the minimum lateral area of a complex structured coating in order for the occurrence of induced drying is presented.

* Corresponding author.

E-mail address: oteschke@ifi.unicamp.br (O. Teschke).

After calculating the minimum lateral area per unit volume necessary to induce drying structured coating was fabricated, its lateral area measured and compared to the value given by Eq. (1). In recent work [14], the top surface of immersed coatings was mapped to evaluate the interaction of water with the coating surface and to determine the effectiveness in supporting water away from the coating base. The contact area between the top surface and the water was measured using a scanning electron microscopy (SEM) and confocal Raman microscopy (CRM). The agreement between the contact area given by the Cassie–Baxter equation and the contact area calculated from the contact points in CRM images was shown to be better than 3%. Capillary evaporation was also investigated recently [15] by observing the time variation of nanochannel profiles inscribed on ice layers on mica substrates under ambient conditions. More recently CRM depth scan was employed to map water and air spatial distributions in hydrophobic films [16].

The film fabricated process is the following: poly(ethyl 2-cyanoacrylate) (PECA) films were prepared on flat glass surfaces via vapor deposition by polymerization of commercial ethyl-2-cyanoacrylate glue (Super Bonder®). The composition of the glue was >90% ethyl-2-cyanoacrylate, <10% polymethyl methacrylate and <10% stabilizers, which includes 1,4-dihydroxybenzene (hydroquinone). Glass slides (1×2 cm) used as substrates were cleaned with isopropyl alcohol and dried under an argon flux. The clean glass substrates were immersed for approximately 10 s in a 25% w/w ammonium hydroxide aqueous solution, a film was then formed on the glass and immediately placed in a Petri dish containing ~200 mg of cyanoacrylate glue. During the fuming process, the reaction times (10 min) were kept constant and the polymerization temperature was varied from 25 °C up to 118 °C. The measured thicknesses of the PECA coating varied from 300 μm to 1 mm.

The characterization of the fabricated film structure is described next: Raman spectra were recorded on a commercial confocal Raman microscope (CRM 200, WiTec, Germany) using an intensity-stabilized single-mode He–Ne laser system (Melles-Griot) (usually $I_{\text{max}} = 15$ mW). Laser radiation was coupled to the microscope via a single-mode fiber. Optical components (filters, gratings, and lenses) were adapted to the appropriate wavelength. The details of the Raman spectra are as follows: $\lambda_{\text{cyanoacrylate}} = 2970$ cm^{-1} , $\lambda_{\text{water}} = 3400$ cm^{-1} and integration time = 0.25 s. Raman spectral imaging used an objective Nikon 60x, NA = 0.8 and excitation 612 nm. Then the substrates containing the organic films prepared under the conditions specified above were fixed in a metallic sample-holder and coated with a thin layer of gold (60 nm) using a Sputtering System AJA ATC 1300-F. The fragments were also observed by using an SEM Leica LEO 440i with digital imaging magnification up to 300,000 \times , provided by secondary electrons, back-scattered electrons and specimen current measurement detectors, operating at a tension of 20 kV.

Two structures of coating were investigated. Initially coatings deposited on glass coverslips were polymerized at a 25 °C for 10 min and the measured contact angle for this coating was ~100° [14]. The water immersed glass coverslips/coating interface was then imaged in a CRM (Fig. 1a). A SEM image of this structure is depicted in Fig. 1b. The measured diameter of the observed structures in Fig. 1a and b was ~4 μm , and the corresponding Raman depth scan image is depicted in Fig. 1c. The resolution of the CRM depth scan image is probably associated with the fact that the detector collects radiation from approximately the extent of the confocal parameter (few micron). In order to determine this resolution the glass coverslips/coating interface was depth

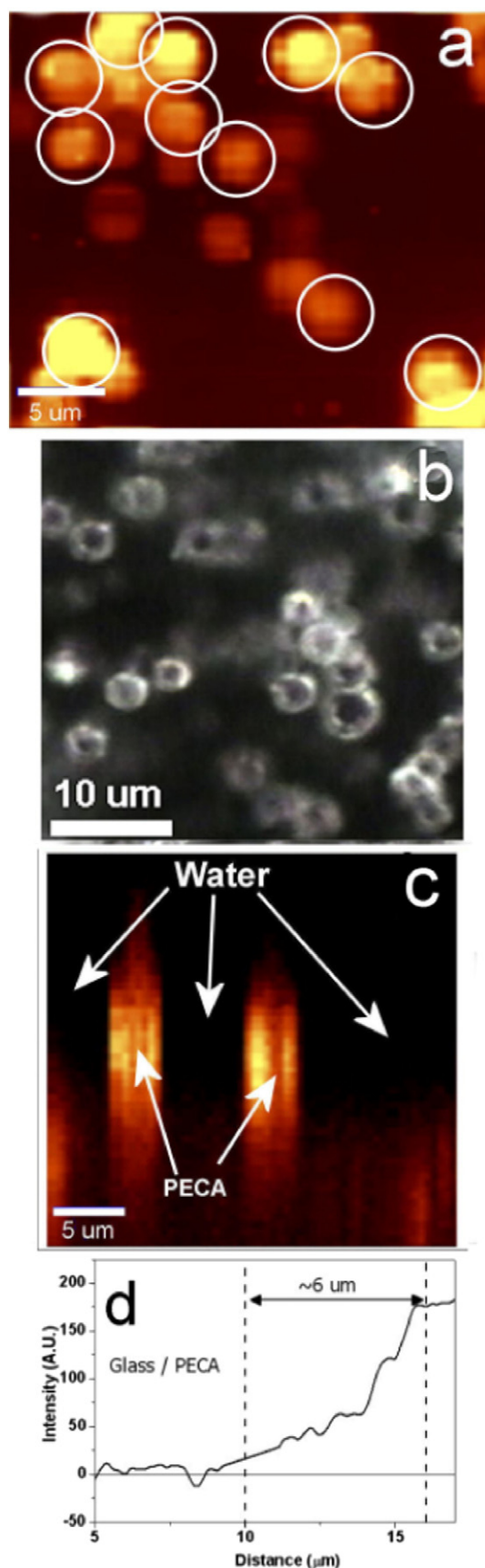


Fig. 1. (a) CRM image of a structure formed by PECA cylinders with diameters of ~4 μm , (b) SEM image showing the PECA cylinders, (c) depth scan images showing cylinder height of ~10 μm . The water occupies the region indicated by a black color and PECA by a yellow reddish color and (d) depth scan profile showing glass/PECA interface. The resolution at interface is indicated by the step width in the figure (~6 μm).

scan imaged (Fig. 1d). The resolution of the images is given by the step length in the depth scan profile ($\sim 6 \mu\text{m}$) as shown in Fig. 1d. The measured height of the cylinder shown in Fig. 1c was $\sim 10 \mu\text{m}$ and it is approximately twice the resolution in the Z-direction. This structured mat immersed in water does not show exclusion liquid layer regions since the interfacial layer is occupied either by water or PECA.

Then more structured deposits were fabricated by further improvements of the deposition technique, obtained by a polymerization at 118°C during 10 min which resulted in hydrophobic coatings with a contact angle of $\sim 160^\circ$. This structure was imaged by SEM and the result is shown in Fig. 2. The rings of PECA fibers are densely intertwined, forming strands in this highly hydrophobic coating. The top surface in contact with coating is indicated by yellow circles. Large amplification SEM images of these structures are shown in Fig. 3a and b. Observe that this structure of ring fibers is formed by spherulites with diameters of $\sim 0.3 \mu\text{m}$.

Fig. 4 shows a CRM depth profile image of the superhydrophobic ($\theta \sim 160^\circ$) ring structure of a PECA coating polymerized at 118°C shown in Figs. 2 and 3 and now immersed in water. The top region, indicated by 1, corresponds to the flooded volume of the coating. Region indicated by 2 is occupied by water and water vapor and corresponds to a transition region. The region corresponding to a total dewetted is labeled 3 in the figure. The spatial distribution of the PECA structure (peak at 3000 cm^{-1}) inside the mat is indicated by 4 and 5. Depth distribution profiles are not fully reliable quantitatively because of the potential boundary refraction error, which introduces depth broadening into the response kernel at distances of a few microns. However, it is still possible to identify a transition (in the focus depth) in which the Raman spectrum switches from being dominated by the features of the water broad line ($3000\text{--}3500 \text{ cm}^{-1}$) (regions 1 and 2) to being dominated by the features of PECA (Raman lines shown in spectrum 4 and 5 in region 3).

The next step was to characterize the coating fiber structure by measuring the nanofiber and microring diameters, the water/coating contact area and the empty space volume between structural features. The spherulite diameter is shown in Fig. 3; for an ensemble of coatings we estimated the numbers of spherulites per unit volume by counting their numbers in coating/water interfaces using SEM images (counts/ m^2) as one shown in Fig. 2. The ensemble was formed by batches each with 5 coating deposited on separated substrates.

The sources of error in the proposed technique is: The determination of the number of points in top surface (liquid/coating interface). Fig. 2 shows 44 contact points at the top surface of the coating characterized

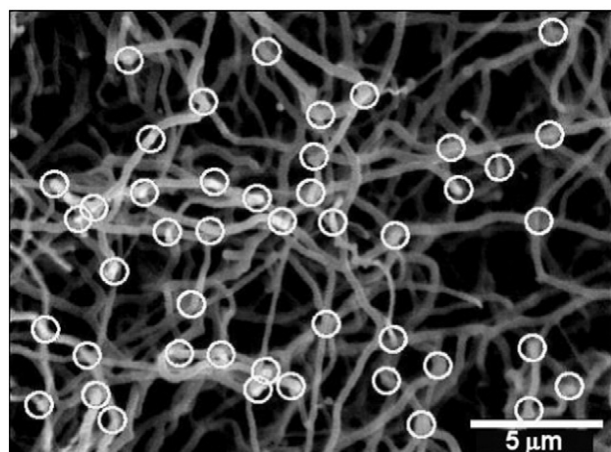


Fig. 2. SEM image of a PECA coating polymerized at a $\sim 118^\circ\text{C}$ and with a contact angle of $\sim 160^\circ$. The fibers have diameters in the range of 0.2 to $0.6 \mu\text{m}$ and ring diameters of $\sim 5 \mu\text{m}$. Top surface contact with the water layer is indicated by yellow circles.

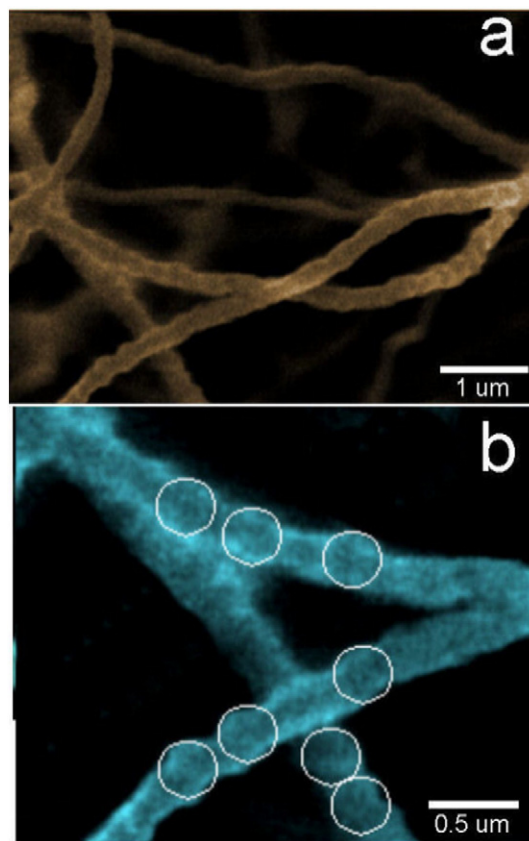


Fig. 3. Large magnification SEM images of a (a) superhydrophobic coating depicted in Fig. 2 showing that the PECA fibers were formed by spherulites and (b) large magnification where spherulites are indicated by white circles (diameter of $\sim 0.3 \mu\text{m}$).

by a sharp bending of fibers. The 44 points are encircled in the figure and it is possible to count 3 more contact points and 3 points that may not be part of the contact area. So an error of 7% is observed in this image. In Fig. 1a the top surface of the coating formed by cylinders shows 11 cylinders and an error of 6%. The other source of error is the measurement of the diameter of the fibers as shown in Fig. 4. We could assume that the spherulites forming the fiber diameters vary from $0.28 \mu\text{m}$ to $0.30 \mu\text{m}$ as indicated in Fig. 3b, resulting in an error of 7%, then the error associated with measuring the contact area is $\sim 10\%$.

In order to calculate the lateral area of the structure we have used SEM images and CRM profiles and we have assumed that fibers are assembled from spherulites, as shown in Figs. 2 and 3b. The profile of the contact region is measured by comparing high resolution SEM images for coatings showing an induced drying and assuming a tridimensional homogeneous distribution of dots forming the interconnected ring structure.

Another parameter that needs to be estimated is the volume of the PECA structure forming the coating layer. The value of the coating volume occupied by PECA fibers was calculated to determine the percentage of the coating that could be occupied by the fluid. The volume occupied by spherulites is given by $\Delta V = N$ (number of spherulites per unit volume) \times volume of spherulites = 0.003 . Then the volume that can be occupied by the fluid is approximately equal to the coating volume $V_{\text{emp}} \approx V_{\text{coating}}$.

In this work, we have built a complex interconnected fiber structure forming superhydrophobic layers where heterogeneous wetting induces drying (see Fig. 4 depth scan image); for PECA coatings characterized by a contact angle of $\sim 160^\circ$ and under ambient conditions ($P = 1 \text{ atm}$, $T = 298 \text{ K}$, $\gamma = 72 \text{ m J/m}^2$, $\Delta\mu = -1.8 \text{ J/mol}$ and $n_l = 0.055 \text{ mol/cm}^3$), the transition is predicted to occur at a threshold value on the order of $\sim 10^6/\text{m}$. Therefore, in the case of a highly

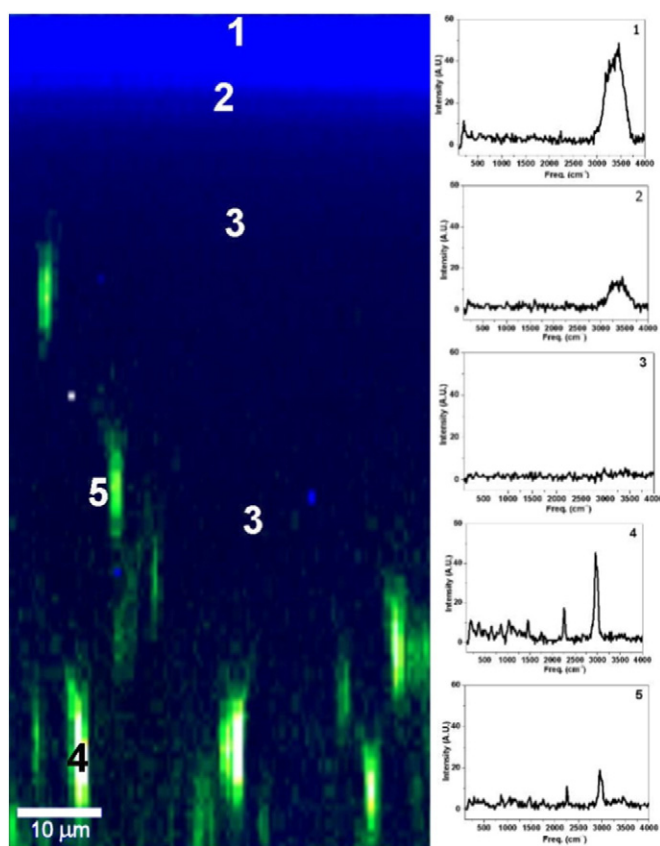


Fig. 4. Depth scan image of the coating shown in Fig. 2 immersed in water. Top region indicated by 1 corresponds to the flooded volume. Region 2 was occupied by water and water-vapor, and corresponds to a transition region. Total dewetted volume is labeled 3. The PECA structure (see diagram at the right) inside the mat is indicated by 4 and 5.

hydrophobic material immersed in water for a ratio of the surface area to the coating volume that is larger than a critical value given by the Kelvin equation ($\sim 10^6/\text{m}$), we would expect liquid to be replaced by vapor.

For a coating with contact angle $\sim 100^\circ$, as shown in Fig. 1a, the PECA fibers forming the structure have diameters of $\sim 4 \mu\text{m}$. By counting their number in the top surface of the film and estimating their height, we have determined the coating lateral area.

The histogram of the lateral area per unit volume of the analyzed coatings is shown in Fig. 5. Coatings that show the empty volume

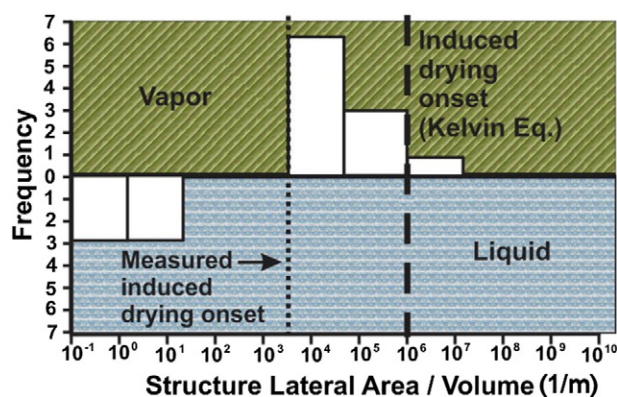


Fig. 5. Histogram of the lateral area per unit volume ($1/\text{m}$) of the probed coatings. Coating with empty volume regions occupied by liquid and vapor is indicated in blue (bottom) and green (top) regions, respectively. The theoretical and experimental values of the induced localized drying onset are indicated by dashed and dotted vertical lines, respectively.

occupied by water are displayed in the blue (lower) region and those occupied by vapor (induced drying regions) are displayed in the green (top) region. The calculated and experimentally measured values of the onset of induced drying are indicated by dashed and dotted vertical lines, respectively. Coatings in which localized drying was not observed typically showed contact angles of $\sim 100^\circ$, and coating in which drying was observed contact angles $\geq 147^\circ$.

The interesting observation is that the crossover of the flooded to the induced drying regime occurs at a value $A/V \sim 10^4/\text{m}$. This crossover is found to vary by two orders of magnitude from the value given by the Kelvin equation (Eq. (1)). Therefore, the induced drying by capillary evaporation for the investigated PECA coatings takes place at a lateral surface/volume ratio far smaller than the value calculated by thermodynamic equilibrium.

The combined analysis of SEM and CRM depth scan images results in a new technique to characterize capillary evaporation that leads to induced drying in immersed, hydrophobic, highly structured coatings. The proposed method is highly reliable for simple coating structures as formed by microcylinders shown in Fig. 1. Capillary drying in highly structured layers reflects the interaction between water and the structured surface; for a detailed discussion of the involved mechanisms see Refs. [3,13,17]. The described fabricated coatings as shown in Fig. 2 are an assembly of two types of disorder, the ring structure orientation and the fiber bending at the interfacial contact region; these two features will affect the size of the hydrophobic units in contact with water due to the induced cooperative effect of the bubbles that cluster and consequently increasing the strength of the hydrophobic interaction, as reported by Weijss [18]. So the water distribution at the coating interface cannot be described as a thermodynamics equilibrium distribution given by Eq. (1). For the real surface, as the one shown in Fig. 2, an unbalanced Young's force will act on the interface and the effect of the coating rugosity spatial variation on the interfacial energy has to be considered [19].

In conclusion we calculated from thermodynamic equilibrium conditions the minimum coating lateral area per unit volume to achieve induced drying. Then we report a new quantitative technique which combines SEM and CRM depth scan images to determine the water exclusion volume inside immersed structured coatings and the lateral area of the structural features. It is possible to show that highly structured hydrophobic coatings favor the vapor phase within the space between its structures when immersed in water. The surface effect ultimately dominates the liquid phase in sufficiently structured features for a lateral area per unit volume larger than $10^4/\text{m}$. This value varies by two orders of magnitude with the value calculated by the thermodynamic equilibrium situation (Kelvin equation). The interfacial water distribution is then modified by the coating contact rugosity spatial variation.

Acknowledgments

The authors are grateful to L. O. Bonugli and J. R. Castro for technical assistance and to the funding support of CNPq 301.282/2009-9.

References

- [1] X. Gong, J. Li, H. Lu, R. Wan, J. Li, J. Hu, H. Fang, A charge-driven molecular water pump, *Nat. Nanotechnol.* 2 (2007) 709–712.
- [2] R. Blossey, Self-cleaning surfaces – virtual realities, *Nat. Mater.* 2 (2003) 301–306.
- [3] F.H. Stillinger, Structure in aqueous solutions of nonpolar solutes from the standpoint of scaled-particle theory, *J. Solut. Chem.* 2 (1973) 141–158.
- [4] P. Ball, Material witness: natural waterproofing, *Nat. Mater.* 8 (2009) 250.
- [5] S. Karpitschka, E. Dietrich, J.R.T. Seddon, J.J.W. Zandvliet, D. Lohse, H. Riegler, Noninvasive optical visualization of surface nanobubbles, *Phys. Rev. Lett.* 109 (2012) 066102–066105.
- [6] C.U. Chan, C.D. Ohl, Total-internal-reflection-fluorescence microscopy for the study of nanobubble dynamics, *Phys. Rev. Lett.* 109 (2012) 174501–174505.
- [7] K. Leung, A. Luzar, D. Bratko, Dynamics of capillary drying in water, *Phys. Rev. Lett.* 90 (2003) 065502–1–4.

- [8] D.M. Spori, T. Drobek, S. Zurcher, N.D. Spencer, Cassie-state wetting investigated by means of a hole-to-pillar density gradient, *Langmuir* 26 (2010) 9465–9473.
- [9] P. Martin, F. Brochard-Wyart, Dewetting at soft interfaces, *Phys. Rev. Lett.* 80 (1998) 3296–3299.
- [10] F. Brochard-Wyart, P.G. Gennest, Dewetting of a water film between a solid and a rubber, *J. Phys. Condens. Matter* 6 (1994) (A9-A12).
- [11] M.L. Blow, J.M. Yeomans, Superhydrophobicity on hairy surfaces, *Langmuir* 26 (2010) 16071–16083.
- [12] A.W. Adamson, *Physical Chemistry of Surfaces*, John Wiley & Sons, Inc, New York, USA, 1990.
- [13] K. Lum, D. Chandler, J.D. Weeks, Hydrophobicity at small and large length scales, *J. Phys. Chem. B* 103 (1999) 4570–4577.
- [14] L.O. Bonugli, M.V. Puydinger dos Santos, E.F. de Souza, O. Teschke, Superhydrophobic polyethylcyanoacrylate coatings. contact area with water measured by Raman spectral images, contact angle and Cassie–Baxter model, *J. Colloid Interface Sci.* 388 (2012) 306–309.
- [15] O. Teschke, J.F. Valente Filho, E.F. de Souza, Drainage kinetics of nanochannels fabricated in water films a few molecules thick on mica at room temperature, *Nanotechnology* 22 (2011) 165304–165312.
- [16] O. Teschke, L.O. Bonugli, M.V. Puydinger dos Santos, Water exclusion layers probed by depth scan confocal Raman microscopy, *Microsc. Microanal.* 19 (2013) 1317–1322.
- [17] D. Chandler, Interfaces and the driving force of hydrophobic assembly, *Nature* 437 (2005) 640–647.
- [18] J.H. Weijs, D. Lohse, Why surface nanobubbles live for hours, *Phys. Rev. Lett.* 110 (2013) 054501–054506.
- [19] O. Teschke, E.F. de Souza, Line tension at high contact angle wetting: contribution to interfacial energy at long distances ($\gg 100$ Å) from the triple line contour, *Chem. Phys. Lett.* 447 (2007) 379–383.